Electronic Supplementary Material (ESI) for Lab on a Chip

Supplementary Information

Dielectrophoresis based continuous-flow nano sorter: fast quality control of gene vaccines

Martina Viefhues, Sonja Wegener, Anja Rischmüller, Martin Schleef, and Dario Anselmetti

Results of DNA single trajectories

During the experiments, two peaks were observed downstream of each ridge (see main text). To identify the species, experiments with single species were performed after separation under identical conditions (see SI figure 1). As expected the larger parental plasmid DNA was deflected at both ridges, whereas the middle-sized miniplasmid DNA was deflected only at the first ridge. Comparing figures 1 a) and b) it becomes clear that the bright structures along the ridge in figure 1 b) is almost the same as in figure 1 a). Thus, those are parental DNA molecules, which adhered to the nanoslit surface during the separation experiment. The *minicircle* DNA passed the first ridge unaffected (not shown).

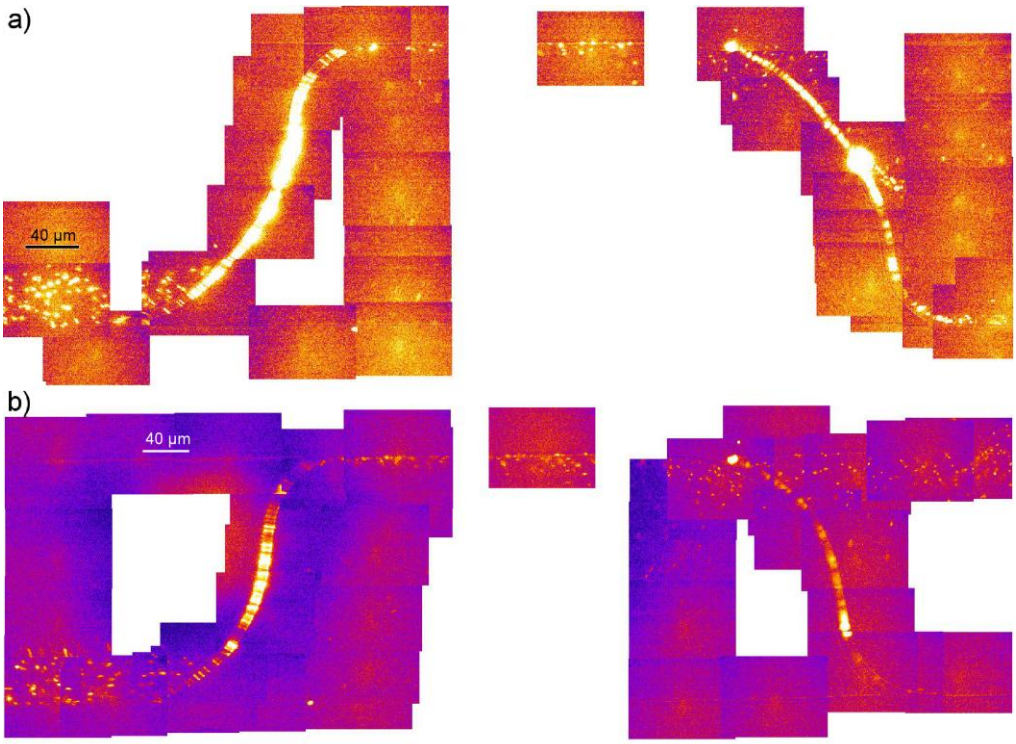

SI figure 1: Results of single species trajectories. a) Collage of the fluorescence microscopy images due to experiment with parental plasmid DNA, exclusively. The parental plasmid DNA migrates along the first and the second ridge towards the other channel wall, respectively. b) Collage of the fluorescence microscopy images due to experiment with miniplasmid DNA, exclusively. The miniplasmid DNA migrates along the

first ridge and escapes at the other channel wall. At the second ridge, the DNA migrates unaffected along the channel.

The different brightness's at the two ridges in figure 1 a) are due to accumulation effects that occur. The DNA migrates along the ridge towards the opposite channel all and accumulates until a "critical" amount of DNA is reached and the DNA escapes continuously (for more information we refer to [39]).

Separation of three nanobead species

Nanobeads of three sizes (100 nm, 60 nm, and 20 nm) were used for proof-of-principle of the multiple-separation. To distinguish between the largest beads (100 nm) and the middle sized beads (60 nm); these were labeled with dyes of different fluorescence emissions (605 nm for 100 nm beads and 480 nm for the 60 nm beads).

A mixture of all three species was continuously injected towards the ridges by applying appropriate dc voltages (see capture SI figure 2). For superimposed ac voltages of 650 Hz at 500 V all of the 100 nm and the 60 nm beads were deflected at the first ridge, whereas the 20 nm beads passed the ridge unaffected and were led into a separate channel. At the second ridge, the 100 nm beads were deflected, too. In contrast to the 60 nm beads that passed the second ridge unaffected. Hence, this device allowed iterative continuous-flow separation of three species.

To characterize the separation efficiency the fluorescence intensities were analyzed up- and downstream of both ridges (see SI figure 2). For the 100 nm beads the evaluation of the fluorescence intensities revealed that at both ridges about 100% of the beads were deflected. On the contrary, the evaluation of the intensity distributions of the 60 nm beads revealed that 60%-90% were deflected at the first ridge, whereas at the second ridge the fluorescence intensity distributions up- and downstream of the ridge were almost the same. Thus, none of the 60 nm beads was deflected at the second ridge.

Due to diffusion the particles stream broadened downstream of the first ridge (see SI figure 3). However, at the second ridge, the 100 nm beads were concentrated by a factor of two, compensating the diffusion effect. The 60 nm beads passed the second ridge unaffected, thus as a wide stream. As a consequence, the separation efficiency was suppressed. To enhance the separation performance the distance between the two ridges was minimized (see main text).

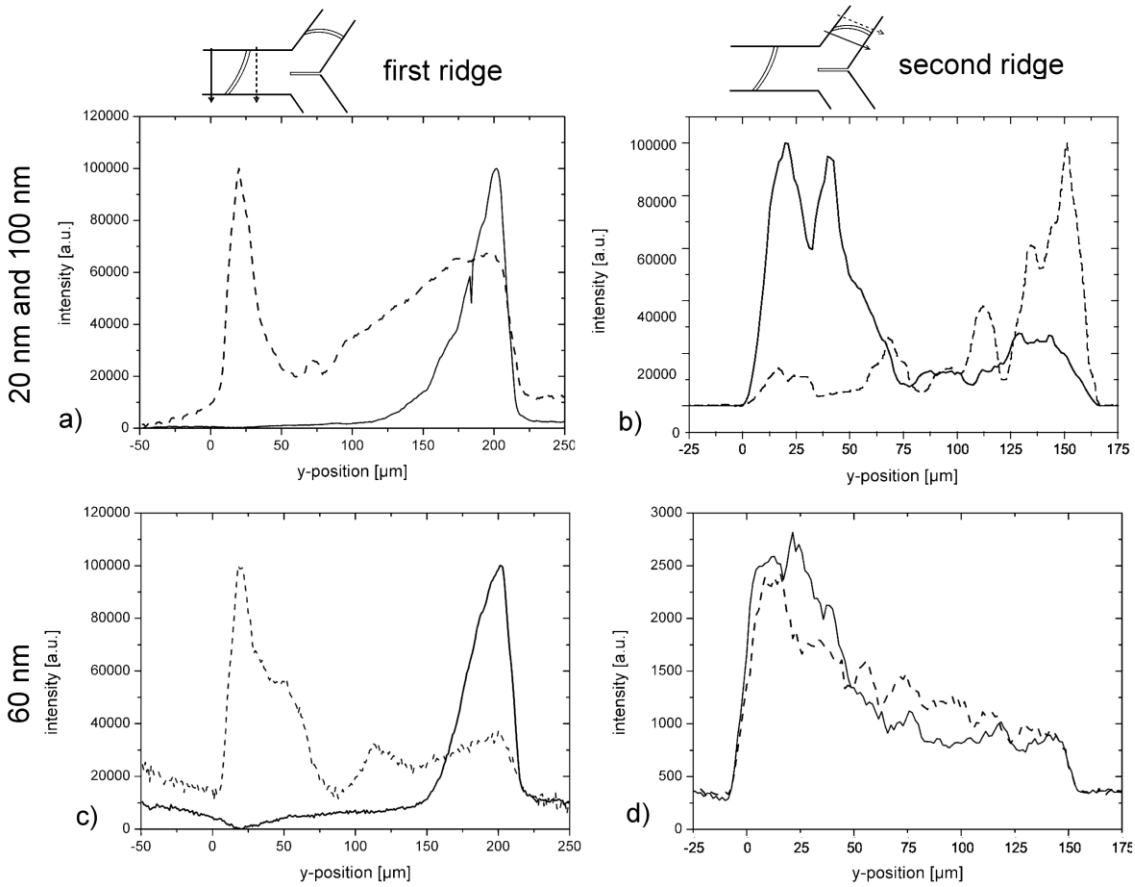

SI figure 2 Results of the multiple-separation of 100 nm, 60 nm, and 20 nm beads. Fluorescence intensity scans up- and downstream of the ridges. The 100 nm, 20 nm and the 60 nm beads were differently stained; unfortunately, they were visible as glowing in the filter of the other beads, respectively. The applied voltages were: 6 V dc and 650 Hz at 500 V ac were applied at electrode 1, 4.5 V dc at electrode 2, 10 V dc at electrode 3; electrodes 4 and 5 were grounded. a) Downstream of the first ridge (200 µm channel width) two peaks appeared depicting the 100 nm and 20 nm beads. The 20 nm peak downstream of the first ridge was broadened due to the unaffected 60 nm beads. The 20 nm beads were induced into a separate outlet. b) The 100 nm beads were fully deflected at the second ridge (150 µm channel width). c) Most of the 60 nm beads (60-90%) were deflected at the first ridge. d) The 60 nm beads passed the second ridge unaffected.

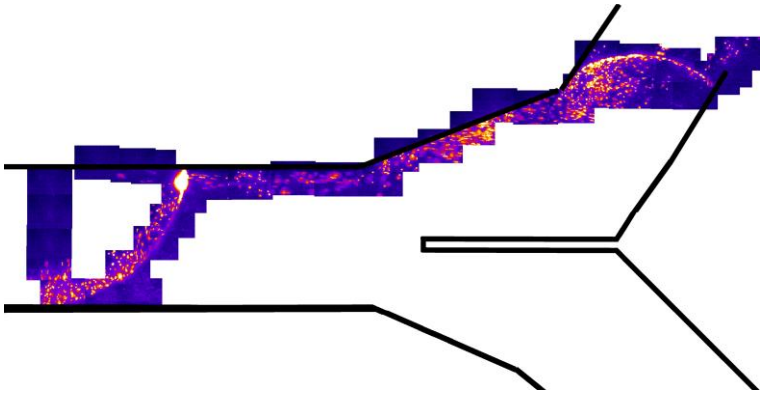

SI figure 3: Fluorescence microscopy images of 100 nm nanobead manipulation. The 100 nm beads were deflected at both ridges. But the species stream significantly broadened between the two ridges. Hence, efficient separation was limited.

Comparison of electric fields within the nanoslits

The multiple-separation was based on varying dielectrophoretic (DEP) potentials at the two ridges, i.e. at the first ridge; the DEP force was stronger than at the second ridge. As a consequence, the largest and the middle-sized species were deflected at the first ridge, whereas at the second ridge the DEP force only trapped the largest species.

The dielectrophoretic potential scales square to the electric field (see main text). Thus, the ratio of the dielectrophoretic potentials is directly accessible by the electric fields at the nanoslits. In SI figure 4 fluorescence microscopy images at the first and the second ridge are depicted. A close look reveals that the longish structure, which is based on the electrophoretic migration of the DNA within the ac electric field, differs significantly: at the first ridge, it spans the whole nanoslit; at the second ridge, it spans only half of the nanoslit. Recalling that the electrophoretic migration of DNA is proportional to the electric field and under the assumption that the shape of the ridge does not influence the electric field strength, the ratio of the electric fields at the two ridges in this device is 2:1 as was predicted theoretically.

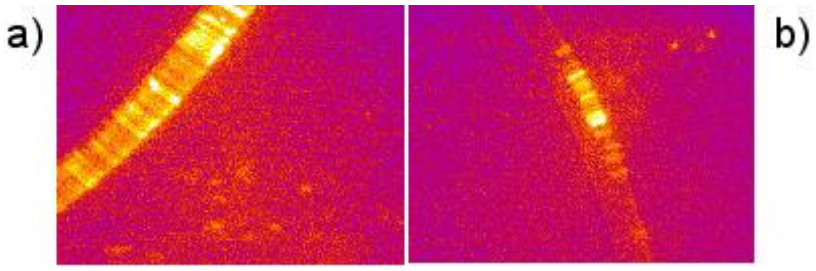

SI figure 4: Comparison of the electric fields within the nanoslits. Fluorescence microscopy images at the two nanoslits. The trapped DNA migrated electrophoretically driven by the ac electric field. a) First ridge, the DNA spans the whole nanoslit. b) Second ridge, the DNA spans half of the ridge. Thus, the ratio of the electric fields is 2:1.